
Appearance of the prolate and the toroidal magnetic field dominated stars – Analytic approach

Kotaro FUJISAWA¹ and Yoshiharu ERIGUCHI²

¹Advanced Research Institute for Science and Engineering, Waseda University, 3-4-1 Okubo, Shinjuku-ku, Tokyo 169-8555, Japan

²Department of Earth Science and Astronomy, Graduate School of Arts and Sciences, University of Tokyo, Komaba, Meguro-ku, Tokyo 153-8902, Japan

*E-mail: fujisawa@heap.phys.waseda.ac.jp

Received 2015 February 27; Accepted 2015 March 27

Abstract

We have analyzed magnetized equilibrium states and showed a condition for appearance of the prolate and the toroidal magnetic field dominated stars by analytic approaches. Both observations and numerical stability analysis support that the magnetized star would have the prolate and the large internal toroidal magnetic fields. In this context, many investigations concerning magnetized equilibrium states have tried to obtain the prolate and the toroidal dominant solutions, but many of them have failed to obtain such configurations. Since the Lorentz force is a cross product of current density and magnetic field, the prolate shaped configurations and the large toroidal magnetic fields in stars require a special relation between current density and the Lorentz force. We have analyzed simple analytical solutions and found that the prolate and the toroidal dominant configuration require non force-free toroidal current density that flows in the opposite direction with respect to the bulk current within the star. Such current density results in the Lorentz force which makes the stellar shape prolate. Satisfying this special relation between the current density and the Lorentz force is a key for appearance of the prolate and the toroidal magnetic field dominated magnetized star.

Key words: stars: magnetars — stars: magnetic fields – stars: rotation

1 Introduction

Anomalous X-ray Pulsars and Soft-Gamma-ray-Repeaters (SGR's) are considered as special classes of neutron stars, i.e. magnetars (Thompson & Duncan 1995). According to observations of rotational periods and their time derivatives, magnitudes of global dipole magnetic fields of magnetars reach about 10^{14-15} G. Recently, however, SGR's with weak dipole magnetic fields have been found (Rea et al. 2010, 2012). Their observational characteristics are very similar to those of ordinary SGR's but their global dipole magnetic fields are much weaker than those of ordinary magnetars. It might be explained by a possibility that such SGR's with small magnetic

fields hide large toroidal magnetic fields under their surfaces and drive their activities by their internal toroidal magnetic energy (Rea et al. 2010). Recent X-ray observation of magnetar 4U 0142+61 also implies the presence of large toroidal magnetic fields and the possibility of prolate-shaped neutron star (Makishima et al. 2014). By considering possible growth of magnetic fields of magnetars during proto-magnetar phases, strong differential rotation within proto-magnetars would amplify their toroidal magnetic fields (Duncan & Thompson 1992; Spruit 2009). Therefore, it would be natural that some magnetars sustain large toroidal magnetic fields inside.

The large toroidal fields are required from the stability anal-

yses of magnetic fields. Stability analyses have shown that stars with purely poloidal fields or purely toroidal fields are unstable (Markey & Tayler 1973; Tayler 1973). Stable magnetized stars should have both poloidal and toroidal magnetic fields. Moreover, the toroidal magnetic field strengths of the stable magnetized stars have been considered to be comparable with those of poloidal components (Tayler 1980). However, we have not yet known the exact stability condition and stable magnetic field configurations, because it is too difficult to carry out stability analyses of stars with both poloidal and toroidal magnetic fields.

Nevertheless, stabilities of magnetic fields have been studied by performing dynamical simulations. Braithwaite & Spruit (2004) showed that twisted-torus magnetic field structures are stable magnetic field configurations on dynamical timescale. Stabilities of purely toroidal magnetic field configurations or purely poloidal magnetic field configurations have been studied in the Newtonian framework (Braithwaite 2006, 2007) and in the full general relativistic framework (Kiuchi et al. 2011; Lasky et al. 2011; Ciolfi et al. 2011; Ciolfi & Rezzolla 2012). Braithwaite (2009) and Duez et al. (2010) have found a stability criterion of the twisted-torus magnetic fields. It could be expressed as

$$\alpha \frac{\mathcal{M}}{|W|} < \frac{\mathcal{M}_p}{\mathcal{M}} \leq 0.8, \quad (1)$$

where $\mathcal{M}/|W|$ is the ratio of the total magnetic energy to the gravitational energy. $\mathcal{M}_p/\mathcal{M}$ is the ratio of the poloidal magnetic field energy to the total magnetic field energy. α is a certain dimensionless factor of order of 10 for main-sequence stars and of order 10^3 for neutron stars. The ratio of $\mathcal{M}/|W|$ is a small value ($\sim 10^{-5}$) even for magnetars. Therefore, the criterion becomes

$$0.2 \leq \frac{\mathcal{M}_t}{\mathcal{M}} \lesssim 0.99, \quad (2)$$

where \mathcal{M}_t is the toroidal magnetic field energy. Stellar magnetic fields would be stable even for toroidal magnetic field dominated configurations. Therefore, it is very natural that the toroidal magnetic field strength of the stable stationary magnetized stars are comparable with or larger than those of poloidal component.

Until recently, however, almost all numerically obtained equilibrium configurations for stationary and axisymmetric stars have only small fractions of toroidal magnetic fields, typically $\mathcal{M}_t/\mathcal{M} \sim 0.01$, even for twisted-torus magnetic field configurations in the Newtonian gravity (Tomimura & Eriguchi 2005; Yoshida & Eriguchi 2006; Yoshida et al. 2006; Lander & Jones 2009; Lander et al. 2012; Fujisawa et al. 2012; Lander 2013, 2014; Bera & Bhattacharya 2014; Armaza et al. 2014), in general relativistic perturbative solutions (Ciolfi et al. 2009; Ciolfi et al. 2010), and general relativistic non-perturbative solutions under both simplified relativistic gravity (Pili et al. 2014)

and fully relativistic gravity (Uryū et al. 2014). All of them do not satisfy the stability criterion mentioned above.

On the other hand, there appeared several works which have successfully obtained the stationary states with strong toroidal magnetic fields by applying special boundary conditions. Glampedakis et al. (2012) obtained strong toroidal magnetic field models imposing surface currents on the stellar surface as their boundary condition. Duez & Mathis (2010) imposed the boundary condition that the magnetic flux on the stellar surface should vanish. Since the magnetic fluxes of their models are zero on the stellar surfaces, all the magnetic field lines are confined within the stellar surfaces. They obtained configurations with strong toroidal magnetic fields which are essentially the same as those of classical works by Prendergast (1956), Woltjer (1959a, 1959b, 1960) and Wentzel (1960, 1961) and recent general relativistic works by Ioka & Sasaki (2004) and Yoshida et al. (2012).

It is very recent that Fujisawa & Eriguchi (2013) have found and shown that the strong toroidal magnetic fields within the stars require the non force-free current or surface current which flows in the opposite direction with respect to the bulk current within the star. Such oppositely flowing currents can sustain large toroidal magnetic fields in magnetized stars. It is also very recent that Ciolfi & Rezzolla (2013) have obtained stationary states of twisted-torus magnetic field structures with very strong toroidal magnetic fields using a special choice for the toroidal current. Their toroidal currents contain oppositely flowing current components and result in the large toroidal magnetic fields, although their paper does not explain the physical meanings for appearances of such oppositely flowing toroidal currents. They also did not show clear conditions for the appearance of the toroidal magnetic field dominated stars.

On the other hand, strong poloidal magnetic fields make stellar shape oblate one (e.g. Tomimura & Eriguchi 2005), but the strong toroidal magnetic field tends to stellar shape prolate one (Haskell et al. 2008; Kiuchi & Yoshida 2008; Lander & Jones 2009; Ciolfi & Rezzolla 2013) Since the Lorentz force is a cross product of the current density and magnetic field, such Lorentz force requires a special relation between the magnetic fields and the current density. At the same time, the large toroidal magnetic fields in stars also need a special relation between current density and Lorentz force. The oppositely flowing toroidal current density is a key to reveal these relations and a condition for appearance of the toroidal magnetic field dominated stars.

We analyze magnetic field configurations and consider the special relations in this paper. We find a condition for the appearance of the toroidal magnetic field dominated stars, which was not described in our previous work (Fujisawa & Eriguchi 2013). In order to show the relations and condition clearly, simplified analytical models are solved and we show examples of the prolate configurations and the large toroidal magnetic fields

within stars. This paper is organized as follows. The formulation and basic equations are shown in Sec. 2. We present analytic solutions and the relations. We also explain the important role of oppositely flowing components of the κ currents for appearance of the prolate shapes and the presence of the large toroidal magnetic fields using the relations in Sec. 3. Discussion and conclusions follow in Sec. 4. In Appendix 1 the deformation of stellar shape and the gravitational potential perturbation are briefly summarized.

2 Formulation and basic equations

Stationary and axisymmetric magnetized barotropic stars without rotation and meridional flows are analyzed in this paper.

Some authors have claimed that there do not exist dynamically stable barotropic magnetized stars (e.g. Mitchell et al. 2015), but in our opinion, their arguments should be applied only to *isentropic barotropes*. The magnetized barotropic stars are well defined concepts apart from the thermal stability or convective stability due to the entropy distributions and/or due to the chemical composition distributions. Thus we will investigate *mechanical equilibrium states* of traditionally defined barotropes (e.g., Chandrasekhar & Prendergast 1956; Prendergast 1956) in this paper.

Since for such configurations the basic equations and basic relations are shown, e.g., in Tomimura & Eriguchi (2005) and Fujisawa & Eriguchi (2013), we show the basic equations and basic relations briefly.

The stationary condition for the configurations mentioned above can be expressed as:

$$\int \frac{dp}{\rho} = -\phi_g + \int \mu(\Psi) d\Psi + C, \quad (3)$$

where ρ , p , ϕ_g and C are the density, the pressure, the gravitational potential of the star and an integral constant, respectively. Ψ is the magnetic flux function. μ is an arbitrary function of Ψ . The magnetic flux is governed by

$$\Delta^* \Psi = -4\pi r \sin \theta \frac{j_\varphi}{c}. \quad (4)$$

where

$$\Delta^* = \left(\frac{\partial^2}{\partial r^2} + \frac{1}{r^2} \frac{\partial^2}{\partial \theta^2} - \frac{1}{r^2} \frac{\cos \theta}{\sin \theta} \frac{\partial}{\partial \theta} \right), \quad (5)$$

and j_φ is a φ -component, i.e. the toroidal component, of the current density. The spherical coordinates (r, θ, φ) are used.

From the integrability condition of the equation of motion, the axisymmetry and the stationarity, the following relations are derived:

$$\frac{j}{c} = \frac{1}{4\pi} \frac{d\kappa}{d\Psi} \mathbf{B} + \rho r \sin \theta \mu(\Psi) \mathbf{e}_\varphi, \quad (6)$$

$$\kappa = \kappa(\Psi), \quad (7)$$

where \mathbf{j} and \mathbf{B} are the current density and the magnetic field,

respectively, and κ is another arbitrary function of Ψ . It would be helpful to note that the above relation for κ was found by Mestel (1961) and Roxburgh (1966). Although $\kappa(\Psi)$ is exactly a function of the magnetic flux function only in stationary and axisymmetric system (Braithwaite 2009), Braithwaite (2008) showed that the function $\kappa(\Psi)$ during the dynamical evolution of magnetized configurations is nearly conserved even for non-axisymmetric systems.

Since the function κ and the φ -component of the magnetic field B_φ is related as

$$\kappa(\Psi) = r \sin \theta B_\varphi, \quad (8)$$

the toroidal current density can be expressed as:

$$\frac{j_\varphi}{c} = \frac{1}{4\pi} \frac{\kappa(\Psi) \kappa'(\Psi)}{r \sin \theta} + \rho r \sin \theta \mu(\Psi). \quad (9)$$

Under our assumption that the magnetic field energy is small compared to the gravitational energy ($\mathcal{M}/|W| < 10^{-5}$) in this paper, the influence of the magnetic fields can be treated as a small perturbation to a spherical star. Therefore, we assume that the stellar configurations are sphere and that the density profile depends only on r , i.e. $\rho = \rho(r)$. For such situations, we can obtain analytical solutions easily. Noted that self-consistent approaches such as Tomimura & Eriguchi (2005), would reveal some differences in the magnetic field solutions. In self-consistent approaches, we need to calculate both magnetic fields and matter equations iteratively. The stellar shape is no longer sphere and the stellar configuration affects the magnetic field configuration. However, our result in this paper is simple and might be important for both perturbative and self-consistent approaches.

3 Spherical models with weak magnetic fields

Our aim in this paper is investigating the condition for appearance of the toroidal magnetic field dominated star analytically. Noted that our solutions of Ψ themselves are classical and not new ones, but we use the solutions in order to show the special condition clearly.

3.1 Green's function approach and analytical solutions

We follow mostly the formulation of the classical works (Chandrasekhar & Prendergast 1956; Prendergast 1956; Woltjer 1959a; Woltjer 1959b, 1960; Wentzel 1960, 1961) and the recent analytical works (Broderick & Narayan 2008; Duez & Mathis 2010; Fujisawa & Eriguchi 2013). In order to obtain analytical solutions, we choose the functional forms as follows:

$$\mu(\Psi) = \mu_0, \quad (10)$$

$$\kappa(\Psi) = \kappa_0 \Psi, \quad (11)$$

where μ_0 and κ_0 are two constants. It should be noted that these functional forms always lead to non-zero surface currents unless magnetic fields are confined inside the star. The surface current induces a Lorentz force at the stellar surface (Lander & Jones 2012). It would be unphysical because the Lorentz force need to be balanced by other physics such as a crust of the neutron star (e.g. Fujisawa & Kisaka 2014). The models relying on a surface current might not be physically realistic. We emphasize that we are not asserting that surface currents themselves are necessarily significant in real stars. The surface current simply provides a mathematically convenient way of describing analytical solutions easily.

By using these functional forms, the toroidal current density can be expressed as:

$$\frac{j_\varphi}{c} = \frac{1}{4\pi} \frac{\kappa_0^2 \Psi}{r \sin \theta} + \mu_0 \rho(r) r \sin \theta. \quad (12)$$

We name the first term κ current $j^{\kappa\varphi}$ (force-free) term and the second term μ current j^μ_φ (non force-free) term, respectively (Fujisawa & Eriguchi 2013). Then, the equation for the magnetic flux becomes as follows:

$$\Delta^* \Psi + \kappa_0^2 \Psi = -4\pi \mu_0 \rho(r) r^2 \sin^2 \theta. \quad (13)$$

It should be noted that this is a linear equation for the magnetic flux function with the inhomogeneous term which contains multipoles less than the quadrupole. If we impose the boundary condition $\Psi = 0$ at the center of the star, Ψ is described as follows (Duez & Mathis 2010; Fujisawa & Eriguchi 2013):

$$\begin{aligned} \frac{\Psi}{\sin^2 \theta} = & K \kappa_0 r j_1(\kappa_0 r) \\ & - 4\pi \mu_0 \kappa_0 \left\{ r j_1(\kappa_0 r) \int_r^{r_s=1} y_1(\kappa_0 r') \rho(r') r'^3 dr' \right. \\ & \left. + r y_1(\kappa_0 r) \int_0^r j_1(\kappa_0 r') \rho(r') r'^3 dr' \right\}. \quad (14) \end{aligned}$$

where we set the stellar radius $r_s = 1$ in this paper. j_1 and y_1 are the spherical Bessel functions of the first kind and the second kind, respectively and K is a coefficient which is determined by a boundary condition of Ψ at the surface. According to the θ -dependency of the inhomogeneous term, we search for solutions of the following form:

$$a(r) \sin^2 \theta \equiv \Psi(r, \theta). \quad (15)$$

Therefore we obtain the solution for $a(r)$ by imposing the boundary condition at the surface and integrating equation (14).

In this paper, we treat spherical polytropes with the polytropic indices $N = 0$ and $N = 1$. As for the configurations of the magnetic fields, we choose two types: (1) closed field models (e.g. Duez & Mathis 2010) and (2) open field models (e.g. Broderick & Narayan 2008). For closed field models, since all magnetic field lines are closed and confined within the star, the magnetic flux must vanish at the stellar surface as follows:

$$a(r_s) = 0. \quad (16)$$

For open field models, since the poloidal magnetic field lines must continue smoothly through the stellar surfaces into the outside, the boundary condition can be expressed as:

$$a(r_s) = - \left. \frac{da(r)}{dr} \right|_{r=r_s}. \quad (17)$$

The density profiles are

$$\rho(r) = \rho_c, \quad (18)$$

for $N = 0$ polytrope and

$$\rho(r) = \rho_c \frac{\sin(\pi r)}{\pi r}. \quad (19)$$

for $N = 1$ polytrope and ρ_c is the central density. We can obtain four different analytical solutions according to four different situations. We name them as $a_{0C}(r)$ ($N = 0$ with closed fields), $a_{0O}(r)$ ($N = 0$ with open fields), $a_{1C}(r)$ ($N = 1$ with closed fields) and $a_{1O}(r)$ ($N = 1$ with open fields).

Since the poloidal magnetic field lines are continuous smoothly at the surfaces for open field models, their external solutions $a^{ex}(r)$ must be expressed as:

$$a^{ex}(r) = \frac{a(r_s)}{r}. \quad (20)$$

It should be noted that the poloidal magnetic fields for closed field models are discontinuous at the surfaces except for solutions with special values of κ_0 , i.e. eigen solutions with corresponding eigenvalues (Broderick & Narayan 2008; Duez & Mathis 2010; Fujisawa & Eriguchi 2013). Therefore, these non-eigen configurations have toroidal surface currents. On the other hand, the toroidal magnetic fields for open field models are always discontinuous because of the choice of the functional form of κ (equation 11). It implies that the open field configurations have non-zero poloidal surface currents.

For non-eigen solutions, the toroidal surface current density can be expressed as follows:

$$\begin{aligned} \frac{j_{\varphi, sur}(\theta)}{c} = & \frac{1}{4\pi} (B_\theta^{ex} - B_\theta^{in}) \Big|_{r=r_s} \\ = & \frac{1}{4\pi r_s \sin \theta} \left(\frac{\partial \Psi^{ex}}{\partial r} - \frac{\partial \Psi^{in}}{\partial r} \right) \Big|_{r=r_s} \\ = & \frac{\sin \theta}{4\pi r_s} \left(\frac{da^{ex}}{dr} - \frac{da^{in}}{dr} \right) \Big|_{r=r_s} \\ = & j_0 \sin \theta, \quad (21) \end{aligned}$$

where superscript in denotes an internal solution and j_0 is a coefficient of the surface current density.

Analytic solutions are obtained by fixing a boundary condition and integrating equation (14). Four different inner solutions ($0 \leq r \leq 1$) can be obtained according to four different situations as follows:

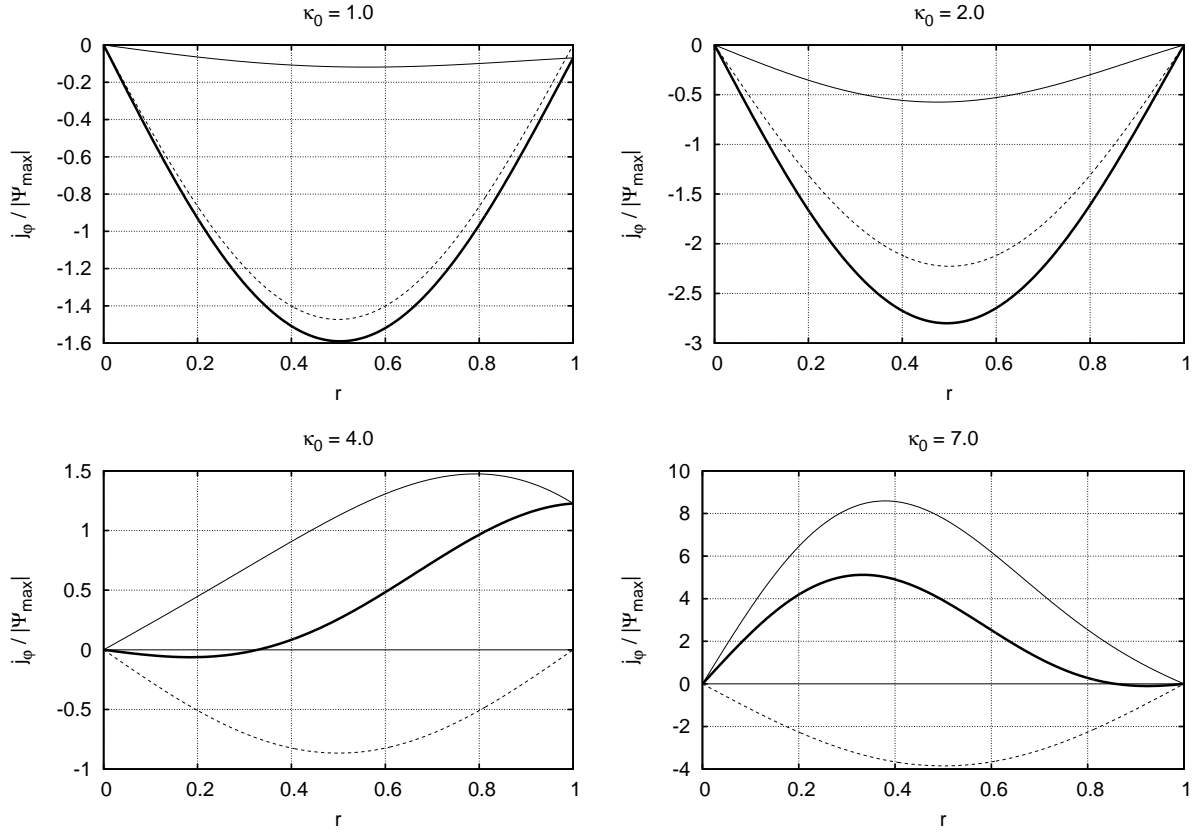


Fig. 1. Distributions of the toroidal current density normalized by the maximum strength of $|\Psi_{\max}|$ are shown along the equatorial plane. Curves with different types denote the behaviors of the total toroidal current density, j_φ/c , (thick solid line), the toroidal κ_0 current density (thin solid line) and the toroidal μ_0 current density (thin dotted line). We set $\mu_0 = -1$ in order to plot these distributions. Left panels show the profiles of solution a_{1O} with $\kappa_0 = 1.0$ and 4.0 and right panels show those of solution a_{1C} with $\kappa_0 = 2.0$ and 7.0 .

$$a_{0C}(r) = 4\pi\mu_0\rho_c \left[\frac{\sin(\kappa_0 r) - \kappa_0 r \cos(\kappa_0 r)}{r\kappa_0^2(\sin \kappa_0 - \kappa_0 \cos \kappa_0)} - \frac{r^2}{\kappa_0^2} \right], \quad (22)$$

$$a_{0O}(r) = 4\pi\mu_0\rho_c \left[\frac{3\{\sin(\kappa_0 r) - \kappa_0 r \cos(\kappa_0 r)\}}{r\kappa_0^4 \sin \kappa_0} - \frac{r^2}{\kappa_0^2} \right], \quad (23)$$

$$a_{1C}(r) = \frac{\mu_0\rho_c}{r(\kappa_0^2 - \pi^2)^2} \left[\frac{8\pi\{\sin(\kappa_0 r) - \kappa_0 r \cos(\kappa_0 r)\}}{\sin \kappa_0 - \kappa_0 \cos \kappa_0} - \{(4\kappa_0^2 - 4\pi^2)r^2 + 8\} \sin(\pi r) + 8\pi r \cos(\pi r) \right], \quad (24)$$

$$a_{1O}(r) = \frac{\mu_0\rho_c}{r(\kappa_0^2 - \pi^2)^2} \left[\frac{(4\pi^3 - 4\pi\kappa_0^2)\{\sin(\kappa_0 r) - \kappa_0 r \cos(\kappa_0 r)\}}{\kappa_0^2 \sin \kappa_0} - \{(4\kappa_0^2 - 4\pi^2)r^2 + 8\} \sin(\pi r) + 8\pi r \cos(\pi r) \right]. \quad (25)$$

The open field models (a_{0O} and a_{1O}) continue to the external solutions ($r \geq 1$) expressed by equation (20). Here it would be helpful to explain several different kinds of characteristic solutions.

First, for $a_{1C}(r)$ solutions there appears a singular solution

at $\kappa_0 = \pi$ (Haskell et al. 2008), while the solution a_{0C} is not singular at $\kappa_0 = \pi$ (Fujisawa & Eriguchi 2013).

Second, although most solutions are accompanied by surface currents, some special solutions have no surface currents. We call such solutions without surface currents as eigen solutions and the values of κ_0 as eigenvalues.

Third, there appear many eigen solutions as the value of κ_0 exceeds the first eigenvalue. We call those eigen solutions as higher-order eigen solutions (see figures in Broderick & Narayan 2008; Duez & Mathis 2010; Yoshida et al. 2012). Those solutions appear when the value of κ_0 exceeds the first eigenvalue of κ_0 for each situation.

Fourth, special solutions with different polytropic indices come to coincide with each other. In other words, those solutions do not depend on the matter distributions. As seen from the expression for the current density, the contribution from the μ current term needs to disappear. It implies that those solutions are determined only by the κ current. Since the κ currents do not contribute to the Lorentz force, these solutions are called as the force-free solutions (Wentzel 1961). The force-free solution is expressed by the following form:

$$a_{ff}(r) = \frac{K}{\kappa_0 r} \{ \sin(\kappa_0 r) - \kappa_0 r \cos(\kappa_0 r) \}. \quad (26)$$

The solution becomes force-free when $\kappa_0 \sim 4.49$ and 7.73 for closed models and when $\kappa_0 = \pi$ and 2π for open field models. (Broderick & Narayan 2008; Fujisawa & Eriguchi 2013).

The toroidal surface current in equation (21) vanishes when the κ_0 is eigenvalue, i.e., for eigen solutions. The lowest eigenvalues are $\kappa_0 \sim 5.76$ for a_{0O} , ~ 7.42 for a_{1c} , ~ 5.76 for a_{0O} and $\kappa_0 \sim 4.66$ for a_{1O} . Hereafter, we focus on solutions with κ_0 less than the lowest eigenvalue. However, our analyses and results could be general and would be valid even when the configurations are higher-order eigen solutions.

In figure 1, distributions of the normalized j_φ/c (thick solid line), the κ current (thin solid line) and the μ current term (dashed line) along the equatorial plane are shown for solutions of a_{1O} (with $\kappa_0 = 1.0, 4.0$, smaller and larger than force-free κ_0 , respectively) and a_{1C} (with $\kappa_0 = 2.0, 7.0$, smaller and larger than force-free κ_0 , respectively.) We have fixed $\mu_0 = -1$ following Fujisawa & Eriguchi (2013) in order to plot these curves.

As seen in upper panels in figure 1, directions (signs) of the μ current, i.e. non force-free current, and the κ current, i.e. force-free current, are the same for solutions with smaller κ_0 . By contrast, for solutions with larger κ_0 (lower panels in figure 1), the μ current flows oppositely to the κ current (Fujisawa & Eriguchi 2013). Moreover, most of the j_φ/c (thick solid line) for solutions with $\kappa_0 = 4.0$ and $\kappa_0 = 7.0$ flows oppositely against the corresponding μ current. Since the sign of the total toroidal current determines the sign of the magnetic flux function (see equation 4), this implies that the sign of $\mu_0\Psi$ for the whole interior region changes from $\mu_0\Psi > 0$ to $\mu_0\Psi < 0$ at the force-free solutions. We calculate many solutions and confirm that the the sign of $\mu_0\Psi$ for the whole interior region changes at the force-free solution. We call the current distribution for which $\mu_0\Psi < 0$ oppositely flowing current.

On the other hand, the surface toroidal currents in the closed field models are always oppositely flowing to the total toroidal currents because of the zero-flux boundary condition equation (16) and the form of the surface current equation (21).

3.2 Deep relation between the toroidal current and the poloidal deformations of stars

As the many previous works pointed out, the toroidal magnetic fields tend to deform stellar shapes prolate, while the poloidal magnetic fields tend to deform them oblate (Wentzel 1960, 1961; Ostriker & Gunn 1969; Mestel & Takhar 1972). These studies used only the magnetic fields in their formulations. The ideal MHD system can be described by using only magnetic fields and one does not need to mention the electrical current density at all. In contrast, we consider both magnetic fields and current density in our calculation. Although these two approaches are equivalent, it is easier to interpret results physi-

cally in terms of the current density. This is the reason why we consider both magnetic fields and current density in this paper. As we have seen in the Sec.3.1, the oppositely flowing toroidal current density ($\mu_0\Psi < 0$) plays a key role for appearance of the large toroidal magnetic fields. The direction of the toroidal current seems to relate to the stellar deformations because the Lorentz force is a cross product of current density and magnetic field. We consider the relation between the toroidal current and the poloidal deformation of stars in this subsection.

In our analytic models, the Lorentz force \mathbf{L} is expressed using the arbitrary function $\mu(\Psi)$ as

$$\begin{aligned} \mathbf{L} &= \left(\frac{\mathbf{j}}{c} \times \mathbf{B} \right) = \rho \nabla \int \mu(\Psi) d\Psi = \rho \mu(\Psi) \nabla \Psi \\ &= \rho \mu_0 \frac{da}{dr} \sin^2 \theta \mathbf{e}_r + 2\rho \mu_0 \frac{a}{r} \sin \theta \cos \theta \mathbf{e}_\theta. \end{aligned} \quad (27)$$

Following Haskell et al. (2008), we consider the stellar quadrupole deformations of $N = 1$ polytropic stars. Haskell et al. (2008) calculated magnetic deformations of polytropic magnetized star with poloidal and toroidal magnetic fields. Although they derived the general forms of the deformations (equation 64, 65 & 67 in their paper), they did not show the analytical expressions of them explicitly. They displayed only a few numerical results in Tab. 1 in their paper. By contrast, we show the analytical solutions of the deformation in order to investigate the condition for appearance of the toroidal magnetic field dominated star.

We assume that the influence of the magnetic fields to the stellar structures are small and that their effects can be treated perturbatively. Due to the effects of the magnetic fields, a certain physical quantity $X(r, \theta)$ is assumed to be expressed as

$$X(r, \theta) = X(r) + \sum_{n=0}^{\infty} \delta X^{(n)}(r) P_n(\cos \theta), \quad (28)$$

where $\delta X^{(n)}$ denotes a small change of order $O(B^2)$ of the quantity X due to the Lorentz force. The angular dependencies are treated by the Legendre polynomial expansions and the coefficient of each Legendre polynomial is expressed as $\delta X^{(n)}(r)$. This expansion is also applied to the Lorentz force as follows:

$$\mathbf{L}(r, \theta) = \sum_{n=0}^{\infty} \mathbf{L}^{(n)}(r) P_n(\cos \theta). \quad (29)$$

From the perturbed equilibrium condition equations, the following relations can be derived:

$$\frac{d\delta p^{(n)}}{dr} + \rho \frac{d\delta\phi_g^{(n)}}{dr} + \delta\rho^{(n)} \frac{d\phi_g}{dr} = L_r^{(n)}, \quad (30)$$

$$\delta p^{(n)} + \rho \delta\phi_g^{(n)} = r L_\theta^{(n)}. \quad (31)$$

Since we are interested in the quadruple deformation, we consider only $n = 2$ components of Lorentz force as follows:

$$L_r^{(2)} = -\frac{2\rho\mu_0}{3} \frac{da(r)}{dr}$$

$$\begin{aligned}
 L_\theta^{(2)} &= -\frac{2\rho\mu_0}{3} \frac{a(r)}{r} \\
 L^{(2)} &\equiv L_r^{(2)} - \frac{d(rL_\theta^{(2)})}{dr} \\
 &= \frac{2\mu_0}{3} \frac{d\rho}{dr} a(r). \tag{32}
 \end{aligned}$$

The change of the stellar surface to the order of the quadrupole term can be expressed as

$$r_d(\theta) = r_s \left\{ 1 + \varepsilon P_2(\cos\theta) \right\} = r_s \left\{ 1 + \frac{\varepsilon}{2} (3\cos^2\theta - 1) \right\}, \tag{33}$$

where $r_d(\theta)$ denotes the deformed surface radius and ε is a small quantity which represents the fraction of the stellar surface along the pole. Following this expression, the stellar shape is prolate for $\varepsilon > 0$ and oblate for $\varepsilon < 0$.

3.2.1 Deformation of $N \neq 0$ polytrope

Using these equations, the quadrupole change of the density is described by:

$$\delta\rho^{(2)} = \left(\frac{d\rho}{dr} \delta\phi_g^{(2)} + L^{(2)} \right) \left(\frac{d\phi_g}{dr} \right)^{-1}. \tag{34}$$

Since the surface of the deformed star is defined by a set of points where the pressure vanishes, i.e.

$$p(r_d(\theta)) = \delta p(r_s) + \varepsilon r_s P_2(\cos\theta) \frac{dp}{dr} \Big|_{r=r_s} = 0, \tag{35}$$

we can derive

$$r_s \varepsilon \frac{d\rho_0}{dr} \Big|_{r=r_s} + \delta\rho^{(2)} \Big|_{r=r_s} = 0, \tag{36}$$

for polytropes with $N \neq 0$. For $N = 0$ polytrope, this equation is reduced to trivial relation $0 = 0$ and so we will treat $N = 0$ polytrope differently as will be shown in the next section. Therefore, the quadrupole surface deformation ε for $N \neq 0$ is obtained by

$$\varepsilon = - \left(\frac{d\rho}{dr} \right)^{-1} \frac{\delta\rho^{(2)}}{r_s} \Big|_{r=r_s}. \tag{37}$$

It is clearly seen that, since $\frac{d\rho}{dr} < 0$ at the surface, the stellar deformation is prolate for $\delta\rho^{(2)} > 0$ and oblate for $\delta\rho^{(2)} < 0$. In our situation, the explicit form of $\delta\rho^{(2)}$ can be expressed as

$$\delta\rho^{(2)} = \frac{d\rho}{dr} \left(\frac{2\mu_0}{3} a(r_s) + \delta\phi_g^{(2)}(r_s) \right) \left(\frac{d\phi_g}{dr} \right)^{-1} \Big|_{r=r_s}, \tag{38}$$

and ε for $N \neq 0$ polytropes becomes as

$$\begin{aligned}
 \varepsilon &= - \left(\frac{2\mu_0}{3} a(r_s) + \delta\phi_g^{(2)}(r) \right) \left(\frac{d\phi_g^{(2)}}{dr} \right)^{-1} \Big|_{r=r_s} \\
 &= \rho \left(\frac{dp}{dr} \right)^{-1} \left(\frac{2\mu_0}{3} a(r_s) + \delta\phi_g^{(2)}(r) \right) \Big|_{r=r_s}. \tag{39}
 \end{aligned}$$

As shown in Appendix 1 the gravitational change for $N = 1$ polytrope can be obtained as

$$\delta\phi_g^{(2)}(x) = \frac{F^{(p)}(x)}{x^3} - \frac{1}{\pi^2} \frac{dF^{(p)}(\pi)}{dx} \Big|_{x=\pi} j_2(x). \tag{40}$$

Thus for $x = \pi$, i.e. on the surface,

$$\delta\phi_g^{(2)}(\pi) = \frac{F^{(p)}(\pi)}{\pi^3} - \frac{3}{\pi^4} \frac{dF^{(p)}}{dx} \Big|_{x=\pi}, \tag{41}$$

where $j_2(\pi) = 3/\pi^2$ is used. Here the function $F^{(p)}(x)$ is defined in Appendix 1. This is a analytic solution of the deformation.

Since the expression for the function $F^{(p)}$ is so complicated, it is not clearly seen the sign of the quantity $(\delta\phi_g^{(2)}(r_s) + 2\mu_0 a(r_s)/3)$ which determines the sign of the quantity ε . In figure 2 we show the behaviors of $-\delta\phi_g^{(2)}(r_s)$ and $-2\mu_0 a(r_s)/3$ against the value of κ_0 . As we have seen, the sign of $\mu_0\Psi$ changes at the force-free solution $\kappa_0 \sim 4.49$ for closed model and $\sim \pi$ for open model. As seen in this figure, the shape change from the effect due to the gravitational change is the same as that from the Lorentz term. Thus the sign of the quantity ε is essentially determined by the sign of the Lorentz term, i.e., the sign of the quantity $\mu_0 a(r_s)$. Since $\rho(r)(dp/dr)^{-1} < 0$, the stellar shape is oblate for $\mu_0\Psi(r, \theta) > 0$ for the whole interior region and prolate for $\mu_0\Psi(r, \theta) < 0$ for the whole interior region as far as the global poloidal magnetic field is dipole. Therefore, the direction of the deformation by Lorentz force is determined by the direction of the non-force free current μ current (equation 12). If the μ current flows oppositely to the magnetic flux ($\mu_0\Psi < 0$), the stellar shape is prolate. If the μ current flows same direction ($\mu_0\Psi > 0$), the stellar shape becomes oblate one. This is a deep relation between the direction of the toroidal current and the poloidal deformations of stars.

In figure 3, the contours of Ψ (dashed curves) and the directions of Lorentz force vectors (arrows) are displayed. It should be noted that directions of the Lorentz forces are totally opposite between models with $\mu_0\Psi(r_s, \theta) > 0$ ($\kappa_0 = 1.0$ and 2.0) and those with $\mu_0\Psi(r_s, \theta) < 0$ ($\kappa_0 = 4.0$ and 7.0)

3.2.2 Deformation for $N = 0$ polytrope

For $N = 0$ polytrope, the gravitational change and the shape change are written as follows as shown in Appendix 2:

$$\delta\phi_g^{(2)} = -\frac{4}{5} \pi G \rho_0 \varepsilon r^2, \tag{42}$$

and

$$\begin{aligned}
 \varepsilon &= \left\{ -\frac{4}{3} \pi G \rho_0 r_s^2 - \left(-\frac{4}{5} \pi G \rho_0 r_s^2 \right) \right\}^{-1} \frac{2\mu_0}{3} a(r_s) \\
 &= -\frac{5\mu_0}{4\pi G \rho_0} a(r_s). \tag{43}
 \end{aligned}$$

Here we use the stationary condition

$$\delta p^{(2)} + \rho_0 \delta\phi_g^{(2)} = r L_\theta^{(2)}, \tag{44}$$

and the surface condition equation (35).

Thus the sign of the quantity ε is exactly determined by the sign of the Lorentz term, i.e., the sign of the quantity $\mu_0 a(r_s)$. The stellar shape is oblate for $\mu_0\Psi(r, \theta) > 0$ for the whole interior region and prolate for $\mu_0\Psi(r, \theta) < 0$ for the whole interior region as far as the global poloidal magnetic field is dipole. The

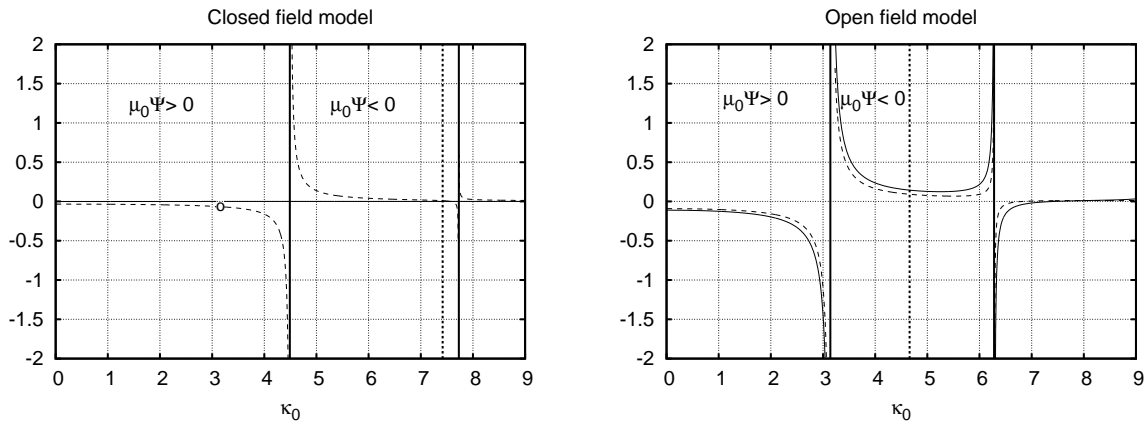


Fig. 2. The values of $-2\mu_0 a(x = \pi)/3$ (thin solid line) and $-\delta\phi_g^{(2)}(x = \pi)$ (thin dashed line) in closed field model (left panel) and open field model (right panel) are plotted. The thick vertical lines denotes force-free limit. The toroidal current densities consist of oppositely flowing flows beyond the dashed thick vertical lines. We set $\mu_0 = -1$ and $\rho_c = 1$ in order to plot these graphs.

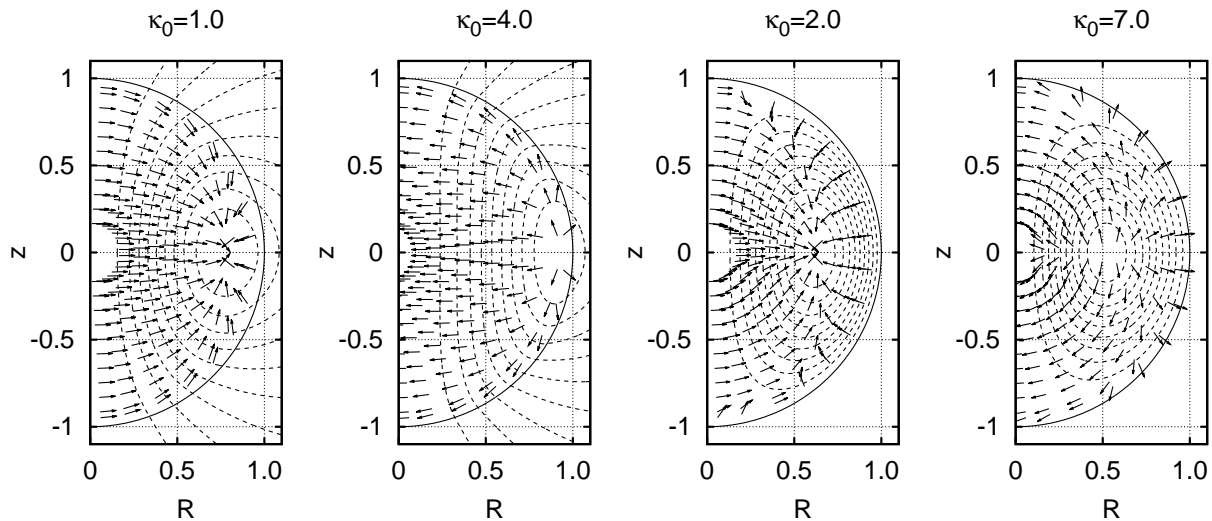


Fig. 3. Poloidal magnetic field structures (dashed curves) and Lorentz force vector fields (arrows) for the open field models ($\kappa_0 = 1.0$, $\kappa_0 = 4.0$) and the closed field models ($\kappa_0 = 2.0$ and $\kappa_0 = 7.0$) are displayed. Vectors only show their directions but are not scaled to their absolute values.

relation between the direction of the μ current and the poloidal deformations of stars is still valid in this case.

3.3 Deep relation between the toroidal current and the strong toroidal magnetic fields

We have found a relation between the oppositely flowing toroidal current density and the Lorentz force in the previous subsection. We consider a relation between the oppositely flowing toroidal current and the strong toroidal magnetic fields in this subsection.

In figure 4, the ratio of the toroidal magnetic field energy \mathcal{M}_t to the total magnetic field energy $\mathcal{M} = \mathcal{M}_p + \mathcal{M}_t$ of each model is plotted for different situations. The solution becomes force-free at the point denoted by the vertical solid lines. The

dashed vertical lines denote the critical values beyond which there arise oppositely flowing κ current structures dominated.

As seen in figure 4, $N = 0$ solutions and $N = 1$ solutions cross at $k_0 \sim 4.49$ and 7.73 for closed field models and $k_0 = \pi$ and 2π for open field models, because the solutions at these points are force-free solutions as mentioned before. The energy ratio is $\mathcal{M}_t/\mathcal{M} \sim 0.5$ when the solutions are the first force-free configurations. Therefore the solutions are divided into two types at the force-free solution. The solution whose κ_0 value is smaller than force-free κ_0 is poloidal dominant configuration, while the solution with larger κ_0 is toroidal dominant configuration. Since the sign of $\mu_0\Psi$ changes at the force-free solution, the solution is poloidal dominant for $\mu_0\Psi(r, \theta) < 0$ for the whole interior region (oppositely flowing current) and the solution is toroidal dominant for $\mu_0\Psi(r, \theta) > 0$ for the whole

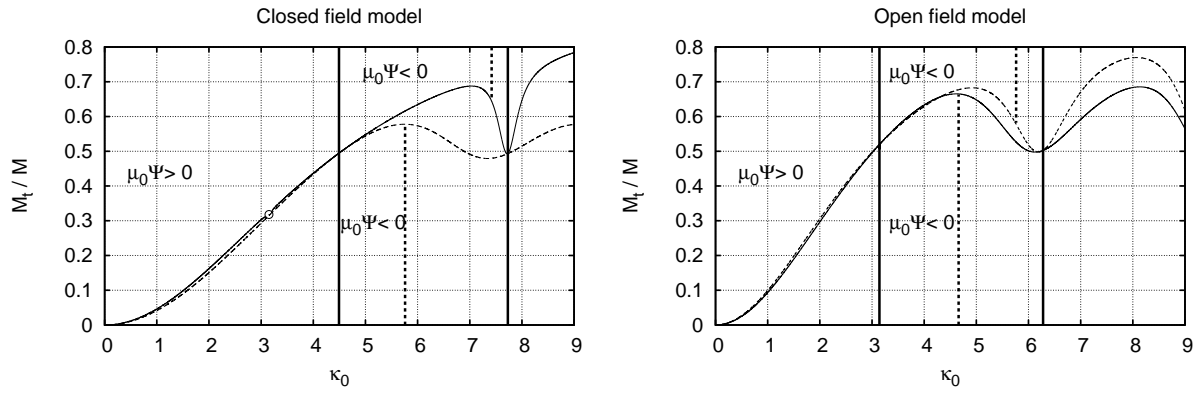


Fig. 4. Energy ratio $\mathcal{M}_t/\mathcal{M}$ is plotted against the value of κ_0 . Closed (left panel) and open (right panel) field solutions are shown. The solid and dashed curves denote $N = 1$ and $N = 0$ solutions, respectively. The vertical solid lines mean force-free solutions: Closed force-free solutions appear at $\kappa_0 \sim 4.49$ and $\kappa_0 \sim 7.73$ and open force-free solutions at $\kappa_0 = \pi$ and $\kappa_0 = 2\pi$. The toroidal current densities are composed of two oppositely flowing components beyond the vertical dashed lines: $\kappa_0 \sim 5.76$ for the a_{0c} solution (dashed curve in left panel), $\kappa_0 \sim 7.42$ for the a_{1c} solution (solid curve in left panel), $\kappa_0 \sim 5.76$ for the a_{0o} solution (dashed curve in right panel) and $\kappa_0 \sim 4.66$ for the a_{1o} (solid curve in right panel). The open circle in the left panel denotes the singular solution for $a_{1c}(r)$.

interior region. The oppositely flowing non-force free current ($\mu_0\Psi(r, \theta) < 0$ for the whole interior region) is required for large toroidal magnetic fields. This is a relation between the toroidal current density and the toroidal magnetic field.

3.4 A situation for appearance of toroidal magnetic field dominated configurations

As we have shown in previous parts in this paper, there are two deep relations between toroidal current, poloidal deformation and strong toroidal magnetic field. One is a relation between the toroidal current and the poloidal deformation of stars in Sec. 3.2. The other is a relation between the toroidal current and the strong toroidal magnetic fields. The important finding in this paper is that the appearance of oppositely flowing non force-free current which fulfills the condition ($\mu_0\Psi < 0$) changes the stellar shape prolate and makes the toroidal magnetic fields toroidal dominant. Therefore, a well-known relation between toroidal dominant magnetic fields and prolate shapes requires the oppositely flowing non force-free toroidal current density. Although our result is very simple and natural, nobody have described explicitly that the oppositely flowing non force-free current density makes the stellar shape prolate. It might be because almost all previous studies treated only magnetic fields and did not pay special attention to current density.

Consequently, we can conclude that a condition for appearance of prolate configurations and the toroidal magnetic field dominated configurations is that the arbitrary function $\mu(\Psi)$ satisfies the following condition:

$$\int \mu(\Psi)d\Psi < 0, \quad (45)$$

for the whole interior region when the functional forms are

equations (10) and (11). Although, exactly speaking, these analyses and conditions are valid within the present parameter settings, our results would be useful for more general situations. This might be naively seen from the contribution of the term $\int \mu d\Psi$ in the stationary condition (equation 3). If this term is negative, it implies that the action of the Lorentz term is opposite to that of the centrifugal force which is expressed by the term $\int \Omega(R)^2 R dR$ and is always positive. In other words, the magnetic forces or Lorentz forces act as if they are the 'anti'-centrifugal forces and therefore shapes of stationary configurations become prolate (see also calculations in Fujisawa & Eriguchi 2014).

Although the condition presented in this paper might not be always correct, we could obtain the large toroidal magnetic fields by employing this criterion for more complicated calculations.

4 Discussion and Summary

4.1 Physical reason for the necessity of appearance of κ currents to realize prolate configurations

In order to get configurations with prolate shapes, we need to include the 'anti'-centrifugal effects or 'anti'-centrifugal potentials. As is easily understood, the anti-centrifugal potentials should behave as decreasing functions from the symmetric axis, or, at least, they must contain decreasing branches which cover wide enough regions to result in effectively anti-centrifugal actions.

For our formulation, the following property is commonly found:

$$\mu > 0 \rightarrow j_\phi^\mu > 0 \rightarrow \Psi > 0 \rightarrow \int \mu d\Psi > 0, \quad (46)$$

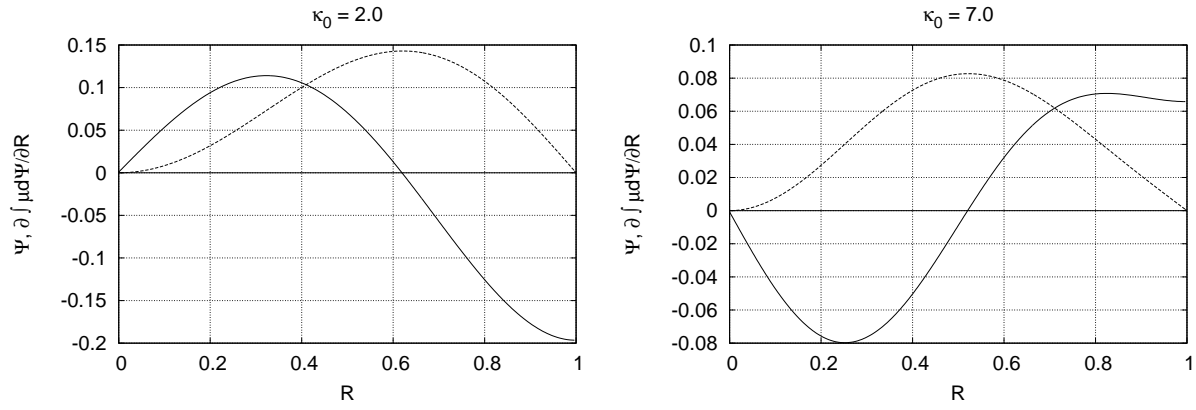


Fig. 5. Distributions of the Ψ (dashed line) and $\partial \int \mu d\Psi / \partial R$ (solid line) of closed field solutions are plotted. The left panel shows the distributions with $\kappa_0 = 2.0$ and $\mu_0 = 1.0$ and the right panel shows those with $\kappa_0 = 7.0$ and $\mu_0 = -1.0$.

and

$$\mu < 0 \rightarrow j_\varphi^\mu < 0 \rightarrow \Psi < 0 \rightarrow \int \mu d\Psi > 0. \quad (47)$$

In addition to these behaviors, for $\Psi > 0$ configurations, the magnetic flux functions increase to the maximum values as the distance from the axis and turn to decrease beyond the maximum point as follows:

$$\frac{\partial \int \mu d\Psi}{\partial R} > 0 \quad \text{for } R < R_{\max}, \quad (48)$$

$$\frac{\partial \int \mu d\Psi}{\partial R} < 0 \quad \text{for } R > R_{\max}, \quad (49)$$

where R_{\max} is the location of the maximum point of the magnetic flux function Ψ (left panel in figure 5).

For $\Psi < 0$ configurations, the magnetic flux functions decrease to the minimum values as the distance from the axis and turn to increase beyond the minimum point:

$$\frac{\partial \int \mu d\Psi}{\partial R} > 0 \quad \text{for } R < R_{\min}, \quad (50)$$

$$\frac{\partial \int \mu d\Psi}{\partial R} < 0 \quad \text{for } R > R_{\min}, \quad (51)$$

where R_{\min} is the location of the minimum point of the magnetic flux function Ψ .

Although there exist decreasing branches for both situations, these decreasing branches cannot overcome the centrifugal effects due to the increasing branches. Therefore, the global configurations with *purely* φ -currents would become oblate shapes.

From this consideration, the anti-centrifugal forces could be realized if the following (necessary) condition is fulfilled:

$$\mu > 0 \quad \text{AND} \quad j_\varphi < 0 \quad \text{AND} \quad \Psi < 0 \quad \text{AND} \quad \int \mu d\Psi < 0, \quad (52)$$

or

$$\mu < 0 \quad \text{AND} \quad j_\varphi > 0 \quad \text{AND} \quad \Psi > 0 \quad \text{AND} \quad \int \mu d\Psi < 0. \quad (53)$$

These conditions could be realized only by including the κ -currents so that the following conditions are satisfied:

$$\mu > 0, \quad j_\varphi^\kappa < 0, \quad j_\varphi^\mu > 0, \quad j_\varphi = j_\varphi^\kappa + j_\varphi^\mu < 0 \quad \text{AND} \quad \Psi < 0, \quad (54)$$

$$\frac{\partial \int \mu d\Psi}{\partial R} < 0 \quad \text{for } R < R_{\min}, \quad (55)$$

$$\frac{\partial \int \mu d\Psi}{\partial R} > 0 \quad \text{for } R > R_{\min}, \quad (56)$$

or

$$\mu < 0, \quad j_\varphi^\kappa > 0, \quad j_\varphi^\mu < 0, \quad j_\varphi = j_\varphi^\kappa + j_\varphi^\mu > 0 \quad \text{AND} \quad \Psi > 0, \quad (57)$$

$$\frac{\partial \int \mu d\Psi}{\partial R} < 0 \quad \text{for } R < R_{\max}, \quad (58)$$

$$\frac{\partial \int \mu d\Psi}{\partial R} > 0 \quad \text{for } R > R_{\max}. \quad (59)$$

The right panel in figure 5 shows the distributions of Ψ and $\frac{\partial \int \mu d\Psi}{\partial R}$ with $\kappa_0 = 7.0$ and $\mu = -1$. As seen in figures 1 and 5, the conditions of the above-mentioned are satisfied undoubtedly. Therefore, the appearance of κ currents j_φ^κ which are oppositely flowing with respect to the μ currents j_φ^μ and at the same time whose magnitudes are large enough to overcome the μ currents are required to realize prolate shapes.

4.2 Twisted-torus configurations with large toroidal magnetic fields

Almost all previously carried out investigations for magnetized equilibrium states having twisted-torus magnetic fields had failed to obtain toroidal magnetic field dominated ($\mathcal{M}_t > \mathcal{M}_p$) models. We have found that most models of their works do not satisfy the condition of equation (45) and the magnetized stellar shapes are oblate due to the μ current term. The κ term in those works has been chosen as follows:

$$\kappa(\Psi) = \kappa_0(\Psi - \Psi_{\max})^{k_1+1} \Theta(\Psi - \Psi_{\max}), \quad (60)$$

where, k_1 is a constant and Θ is the Heaviside step function and Ψ_{\max} is the maximum value of Ψ on the last closed field line within the star. Since the current density of this functional

form vanishes at the stellar surface, there exist no surface current and exterior current density. This functional form was used by Tomimura & Eriguchi (2005) for the first time and results in the twisted-torus configurations. The same choice for the κ has been employed by many authors (e.g. Yoshida & Eriguchi 2006; Yoshida et al. 2006; Kiuchi & Kotake 2008; Lander & Jones 2009; Ciolfi et al. 2009; Ciolfi et al. 2011; Fujisawa et al. 2012; Glampedakis et al. 2012; Lander et al. 2012; Fujisawa et al. 2013; Fujisawa & Eriguchi 2013; Lander 2013, 2014). While the functional form $\mu(\Psi) = \mu_0$ (constant) has been used in many investigations, Fujisawa et al. (2012) and Fujisawa et al. (2013) used a different functional form as

$$\mu(\Psi) = \mu_0(\Psi + \epsilon)^m, \quad (61)$$

where m and ϵ are positive constants. They have obtained highly localized poloidal magnetic field configurations using this type of functional form. However, their works did not satisfy the condition of equation (45) and did not obtain models with large toroidal magnetic fields.

Recently, Ciolfi & Rezzolla (2013) have adopted a perturbative approach and succeeded in obtaining magnetized equilibrium states with twisted-torus magnetic fields whose toroidal fields are large. Their functional form of κ is

$$\kappa(\Psi) = \kappa_0 \Psi (|\Psi/\Psi_{\max}| - 1) \Theta(|\Psi/\Psi_{\max}| - 1). \quad (62)$$

On the other hand, the functional form of μ is

$$\mu(\Psi) = c_0 [(1 - |\Psi/\Psi_{\max}|)^2 \Theta(1 - |\Psi/\Psi_{\max}|) - \bar{k}] + X_0 \kappa(\Psi) \frac{d\kappa(\Psi)}{d\Psi}, \quad (63)$$

where $c_0, \bar{k} (> 0)$ and X_0 are constants. The toroidal magnetic field is confined within the last closed field line in these functional forms. Outside the toroidal magnetic field region, the function κ vanishes and μ becomes

$$\mu(\Psi) = c_0 [(1 - |\Psi/\Psi_{\max}|)^2 - \bar{k}]. \quad (64)$$

Since the first term and the second term are positive and negative, respectively, this function with larger \bar{k} tends to satisfy the condition of equation (45). As they noted, larger values of \bar{k} result in larger energy ratios $\mathcal{M}_t/\mathcal{M}$. As the value of k increases, the energy ratio $\mathcal{M}_t/\mathcal{M}$ increases and the stellar shape becomes more prolate in general (see Tab.1 in Ciolfi & Rezzolla 2013). However, they assumed that the magnetic field configuration is purely dipole but their functional forms and toroidal current density distribution are far from dipole one (see bottom panels of figure 2 in Ciolfi & Rezzolla 2013). Non-perturbative studies with higher order components were unable to reproduce their results and found contradictory results (Bucciantini et al. 2015). We need to calculate magnetic field configurations with higher order components for large toroidal models by using non-perturbative methods in the future.

The condition of equation (45) itself is valid when a star is

barotropic. However, the relation between oppositely flowing toroidal current density and prolate shape is very simple and natural when a star is non-barotropic. Therefore, this condition is also useful for recent perturbative non-barotropic solutions (Mastrano et al. 2011; Mastrano & Melatos 2012; Akgün et al. 2013; Yoshida 2013). We also need to investigate non-perturbative non-barotropic magnetized equilibrium states in the future.

4.3 Summary

In this paper, we have obtained four analytic solutions with both open and closed magnetic fields for spherical polytropes with weak magnetic fields.

Using the obtained solutions we have discussed the situations for which the prolate equilibrium states and the toroidal magnetic field dominated configurations appear. The main finding in this paper is that the appearance of the prolate shapes and the toroidal magnetic field dominated states are accompanied by the appearance of oppositely flowing κ currents with respect to the μ current. This situation seems to be related to the condition for the non force-free toroidal current contribution, i.e. $\int \mu(\Psi) d\Psi$, in the stationary state condition equation (3).

Although the appearance of prolate shapes and the occurrence of toroidal magnetic field dominated states cannot be defined quantitatively, the rough qualitative idea about them can be determined by checking the sign of the magnetic field potential, i.e. the quantity $\int \mu(\Psi) d\Psi$.

Of course, the analytic solutions obtained in this paper have been derived under very restricted assumptions. However, as explained in the Discussion, the concept of the 'anti'-centrifugal actions due to the magnetic potentials would be applied to more general situations for the magnetic fields.

Acknowledgments

KF would like to thank the anonymous reviewer for useful comments and suggestions that helped us to improve this paper. This work was supported by Grant-in-Aid for Scientific Research on Innovative Areas, No.24103006.

References

- Akgün, T., Reisenegger, A., Mastrano, A., & Marchant, P. 2013, MNRAS
- Armaza, C., Reisenegger, A., & Valdivia, J. A. 2014, ArXiv e-prints
- Bera, P. & Bhattacharya, D. 2014, MNRAS, 445, 3951
- Braithwaite, J. 2006, A&A, 453, 687
- Braithwaite, J. 2007, A&A, 469, 275
- Braithwaite, J. 2008, MNRAS, 386, 1947
- Braithwaite, J. 2009, MNRAS, 397, 763
- Braithwaite, J. & Spruit, H. C. 2004, Nature, 431, 819
- Broderick, A. E. & Narayan, R. 2008, MNRAS, 383, 943
- Bucciantini, N., Pili, A. G., & Del Zanna, L. 2015, MNRAS, 447, 3278

Chandrasekhar, S. & Prendergast, K. H. 1956, Proceedings of the National Academy of Science, 42, 5

Ciolfi, R., Ferrari, V., & Gualtieri, L. 2010, MNRAS, 406, 2540

Ciolfi, R., Ferrari, V., Gualtieri, L., & Pons, J. A. 2009, MNRAS, 397, 913

Ciolfi, R., Lander, S. K., Manca, G. M., & Rezzolla, L. 2011, ApJ, 736, L6

Ciolfi, R. & Rezzolla, L. 2012, ApJ, 760, 1

Ciolfi, R. & Rezzolla, L. 2013, MNRAS, 435, L43

Duez, V., Braithwaite, J., & Mathis, S. 2010, ApJ, 724, L34

Duez, V. & Mathis, S. 2010, A&A, 517, A58+

Duncan, R. C. & Thompson, C. 1992, ApJ, 392, L9

Fujisawa, K. & Eriguchi, Y. 2013, MNRAS, 432, 1245

Fujisawa, K. & Eriguchi, Y. 2014, MNRAS, 438, L61

Fujisawa, K. & Kisaka, S. 2014, MNRAS, 445, 2777

Fujisawa, K., Takahashi, R., Yoshida, S., & Eriguchi, Y. 2013, MNRAS, 431, 1453

Fujisawa, K., Yoshida, S., & Eriguchi, Y. 2012, MNRAS, 422, 434

Glampedakis, K., Andersson, N., & Lander, S. K. 2012, MNRAS, 420, 1263

Haskell, B., Samuelsson, L., Glampedakis, K., & Andersson, N. 2008, MNRAS, 385, 531

Ioka, K. & Sasaki, M. 2004, ApJ, 600, 296

Kiuchi, K. & Kotake, K. 2008, MNRAS, 385, 1327

Kiuchi, K. & Yoshida, S. 2008, Phys. Rev. D, 78, 044045

Kiuchi, K., Yoshida, S., & Shibata, M. 2011, A&A, 532, A30

Lander, S. K. 2013, Physical Review Letters, 110, 071101

Lander, S. K. 2014, MNRAS, 437, 424

Lander, S. K., Andersson, N., & Glampedakis, K. 2012, MNRAS, 419, 732

Lander, S. K. & Jones, D. I. 2009, MNRAS, 395, 2162

Lander, S. K. & Jones, D. I. 2012, MNRAS, 424, 482

Lasky, P. D., Zink, B., Kokkotas, K. D., & Glampedakis, K. 2011, ApJ, 735, L20

Makishima, K., Enoto, T., Hiraga, J. S., et al. 2014, Physical Review Letters, 112, 171102

Markey, P. & Tayler, R. J. 1973, MNRAS, 163, 77

Mastrano, A. & Melatos, A. 2012, MNRAS, 421, 760

Mastrano, A., Melatos, A., Reisenegger, A., & Akgün, T. 2011, MNRAS, 417, 2288

Mestel, L. 1961, MNRAS, 122, 473

Mestel, L. & Takhar, H. S. 1972, MNRAS, 156, 419

Mitchell, J. P., Braithwaite, J., Reisenegger, A., et al. 2015, MNRAS, 447, 1213

Ostriker, J. P. & Gunn, J. E. 1969, ApJ, 157, 1395

Pili, A. G., Bucciantini, N., & Del Zanna, L. 2014, MNRAS, 439, 3541

Prendergast, K. H. 1956, ApJ, 123, 498

Rea, N., Esposito, P., Turolla, R., et al. 2010, Science, 330, 944

Rea, N., Israel, G. L., Esposito, P., et al. 2012, ApJ, 754, 27

Roxburgh, I. W. 1966, MNRAS, 132, 347

Spruit, H. C. 2009, in Proceedings IAU Symposium, Vol. 259, Cosmic Magnetic Fields: From Planets, to Stars and Galaxies, ed. K. G. Strassmeier, A. G. Kosovichev & J. E. Beckman, 61–73

Tayler, R. J. 1973, MNRAS, 161, 365

Tayler, R. J. 1980, MNRAS, 191, 151

Thompson, C. & Duncan, R. C. 1995, MNRAS, 275, 255

Tomimura, Y. & Eriguchi, Y. 2005, MNRAS, 359, 1117

Uryū, K., Gourgoulhon, E., Markakis, C. M., et al. 2014, Phys. Rev. D, 90, 101501

Wentzel, D. G. 1960, ApJS, 5, 187

Wentzel, D. G. 1961, ApJ, 133, 170

Woltjer, L. 1959a, ApJ, 130, 400

Woltjer, L. 1959b, ApJ, 130, 405

Woltjer, L. 1960, ApJ, 131, 227

Yoshida, S. 2013, MNRAS, 435, 893

Yoshida, S. & Eriguchi, Y. 2006, ApJ, 164, 156

Yoshida, S., Kiuchi, K., & Shibata, M. 2012, Phys. Rev. D, 86, 044012

Yoshida, S., Yoshida, S., & Eriguchi, Y. 2006, ApJ, 651, 462

Appendix 1 Change of the gravitational potential for $N = 1$ polytrope

The gravitational potential perturbation for $N = 1$ polytrope is governed by the quadrupole component of Poisson's equation under two boundary conditions ($\delta\phi_g^{(2)}$ is regular at $r = 0$ and continues the external solution smoothly at $r = r_s$):

$$\frac{d^2\delta\phi_g^{(2)}}{dr^2} + \frac{2}{r}\frac{d\delta\phi_g^{(2)}}{dr} - \frac{6}{r^2}\delta\phi_g^{(2)} = 4\pi G\delta\rho^{(2)}. \quad (\text{A1})$$

Considering the density perturbation expressed by equation (34), this equation can be rewritten as

$$\begin{aligned} \frac{d^2\delta\phi_g^{(2)}}{dr^2} + \frac{2}{r}\frac{d\delta\phi_g^{(2)}}{dr} + \left(\pi^2 - \frac{6}{r^2}\right)\delta\phi_g^{(2)} \\ = 4\pi G\left(\frac{d\phi_g}{dr}\right)^{-1}L^{(2)}(r). \end{aligned} \quad (\text{A2})$$

By introducing the new variable $x = \pi r$, the left-hand side of the equation is reduced to

$$\begin{aligned} \frac{d^2\delta\phi_g^{(2)}}{dx^2} + \frac{2}{x}\frac{d\delta\phi_g^{(2)}}{dx} + \left(1 - \frac{6}{x^2}\right)\delta\phi_g^{(2)} \\ = \frac{4\pi G}{\pi^2}\left(\frac{d\phi_g}{dr}\right)^{-1}L^{(2)}(r). \end{aligned} \quad (\text{A3})$$

The solution to this equation can be obtained by taking the boundary conditions into account as follows:

$$\delta\phi_g^{(2)}(x) = \frac{F^{(p)}(x)}{x^3} - \frac{1}{\pi^2}\frac{dF^{(p)}(\pi)}{dx}\Big|_{x=\pi}j_2(x), \quad (\text{A4})$$

where

$$\begin{aligned} F^{(p)}(x) \\ = -\frac{2}{3}\mu_0 A_1 \frac{\pi^2}{\kappa_0^2(\pi^2 - \kappa_0^2)^2} \left[\{6\pi^2\kappa_0^2 + (\pi^2 - 3\kappa_0^2)\kappa_0^2 x^2\} \sin\left(\frac{\kappa_0}{\pi}x\right) \right. \\ \left. - \frac{\kappa_0}{\pi}x \{6\pi^2\kappa_0^2 + (\pi^2 - \kappa_0^2)\kappa_0^2 x^2\} \cos\left(\frac{\kappa_0}{\pi}x\right) \right] \\ - \frac{2}{3}\mu_0 A_2 \left[\frac{1}{2}x^4 \sin x + \frac{1}{6}\left(\frac{\kappa_0^2}{\pi^2} - 1\right)x^5 \cos x \right]. \end{aligned} \quad (\text{A5})$$

Here the coefficients A_1 and A_2 are defined as

$$A_1 = \frac{8\pi^2\mu_0\rho_c}{(\kappa_0^2 - \pi^2)^2} \frac{1}{(\sin\kappa_0 - \kappa_0\cos\kappa_0)}, \quad (\text{A6})$$

$$A_2 = \frac{4\pi\mu_0\rho_c}{(\kappa_0^2 - \pi^2)^2}, \quad (\text{A7})$$

for $N = 1$ closed configurations and

$$A_1 = -\frac{4\pi^2\mu_0\rho_c}{\kappa_0^2(\kappa_0^2 - \pi^2)} \frac{1}{\sin\kappa_0}, \quad (\text{A8})$$

$$A_2 = \frac{4\pi\mu_0\rho_c}{(\kappa_0^2 - \pi^2)^2}, \quad (\text{A9})$$

for $N = 1$ open configurations.

Appendix 2 Surface change for $N = 0$ polytrope

The change of the gravitational potential due to the change of the surface, i.e. $\varepsilon r_s P_2(\cos\theta)$, can be obtained by

$$\begin{aligned} \delta\phi_g^{(2)}(r) &= -4\pi G\rho_0 \int_0^\pi d\theta' P_2(\cos\theta') \int_{r_s}^{r_s(1+\varepsilon)P_2(\cos\theta')} dr' r'^2 \frac{r^2}{r'^3} \\ &= -\frac{4\pi G\rho_0}{5} r^2 \varepsilon. \end{aligned} \quad (\text{A10})$$